

RESEARCH

Open Access



# Biomaterial-based chitosan nanohydrogel films: combination of *Bistorta officinalis* and Ca-doped carbon dots for improved blood clotting

Hassan Tavakoli<sup>1\*</sup>, Meysam Najafloo<sup>2,3</sup> and Ahmad Yarikhosroushahi<sup>2,3\*</sup>

## Abstract

**Background** Bleeding and traumatic injuries are still a major issue necessitating the development of advanced hemostatic materials that are economical, biocompatible, and effective. Chitosan's (CS) haemostatic and biocompatible properties make it a promising wound-healing material, however, effective cross-linking is essential for appropriate physiochemical properties. In this study, calcium-doped carbon dots (CDs) produced from coriander leaves were used as cross-linking agents to improve the functional performance and structural integrity of nanohydrogel films. Furthermore, extract of the medicinal plant *Bistorta officinalis* (BEX), a traditional medicinal plant with strong hemostatic and antibacterial qualities, was incorporated into the hydrogel matrix.

**Results** Analysis and characterization of the synthesized CDs thoroughly confirmed that they have monodispersed spherical shape, negative zeta potential, and active functional groups which effectively cross-linked the chitosan matrix and increased the mechanical strength and stability of the film. Cytotoxicity and antibacterial results of the final films showed the desired cytocompatibility against Human skin fibroblast (HFF-1 cells) with over 80% viability at the highest concentration and effective antibacterial activity against gram-positive and gram-negative bacteria (further improved by cross-linking with CDs and incorporating BEX), respectively. The incorporation of BEX and CDs in hydrogel films significantly enhanced the film's blood-clotting ability with negligible hemolysis due to blood clotting index and hemolysis tests.

**Conclusions** The findings of this study highlight the potential of biomaterial-based nano hydrogel film, composed of CS cross-linked with CDs and containing BEX, as a promising wound dressing with outstanding biocompatibility, minimal cytotoxicity, enhanced hemostatic efficacy, and strong antibacterial properties.

**Keywords** Nanoparticles, Carbon dots, *Bistorta* extraction, Hydrogels, Chitosan, Blood clotting

\*Correspondence:

Hassan Tavakoli  
hs.tavakoli51@gmail.com  
Ahmad Yarikhosroushahi  
Ayrikh@gmail.com

<sup>1</sup>Department of Chemistry, Faculty of Basic Sciences, Imam Ali University, Imam Khomeini Street, P.O. Box 1317893471, Tehran 1317893471, Iran

<sup>2</sup>Drug Applied Research Center, Tabriz University of Medical Sciences, Golgasht Street, Tabriz 516615731, Iran

<sup>3</sup>Department of Medical Nanotechnology, Faculty of Advanced Medical Sciences, Tabriz University of Medical Sciences, Golgasht Street, Tabriz 516615731, Iran



© The Author(s) 2025. **Open Access** This article is licensed under a Creative Commons Attribution-NonCommercial-NoDerivatives 4.0 International License, which permits any non-commercial use, sharing, distribution and reproduction in any medium or format, as long as you give appropriate credit to the original author(s) and the source, provide a link to the Creative Commons licence, and indicate if you modified the licensed material. You do not have permission under this licence to share adapted material derived from this article or parts of it. The images or other third party material in this article are included in the article's Creative Commons licence, unless indicated otherwise in a credit line to the material. If material is not included in the article's Creative Commons licence and your intended use is not permitted by statutory regulation or exceeds the permitted use, you will need to obtain permission directly from the copyright holder. To view a copy of this licence, visit <http://creativecommons.org/licenses/by-nc-nd/4.0/>.

## Introduction

Traumatic injuries that cause significant bleeding are one of the main causes of death rates worldwide. The skin, being the largest organ in the body, performs various functions and can be susceptible to a range of injuries such as sores, ulcers, burns, and traumatic wounds, which have the potential to cause significant health problems and even death [1]. A wide range of wound-healing and hemostatic materials have been designed, evaluated, and applied to effectively control bleeding, protect the wound surface from infection and secondary damage, and facilitate the wound-healing process [2]. A diverse array of natural and synthetic polymers, possessing distinct physical, chemical, and biological characteristics, have been studied and utilized in the development of novel wound dressings [3, 4].

Synthetic wound-healing methods, despite advancements, face challenges such as short retention time, high costs, low efficacy, and more importantly high toxicity with a high risk of infection and inflammation which can result in cutaneous adverse effects [5]. The limitations of current methods have highlighted the necessity for high-performance and non-toxic alternatives.

Biomaterial-based hydrogels, especially those made from natural precursors such as CS, are being considered as promising candidates due to their successful performance in various important fields of medical science, such as intelligent drug delivery, innovative immunotherapy systems, tissue engineering, and wound healing, according to distinct physicochemical properties [6–12]. Biomaterial-based hydrogels can provide a framework that could be incorporated with different additives to provide a framework for the addition of specific agents such as antimicrobial drugs, growth factors, and other biomacromolecules [4, 13, 14].

CS, a polymer made of carbohydrates obtained from marine sources, due to its unique properties, including biocompatibility, enzymatic degradation capabilities, and antimicrobial effect, is a versatile material for biomedical applications [15–19].

The physicochemical properties of hydrogels are also related to their structural performance such as three-dimensional structure, mechanical stability, swelling rates, and elasticity to provide a suitable protective barrier and act as a framework for the development of an environment that promotes appropriate regeneration [7, 20]. The structural performance of hydrogels is significantly influenced by the choice of crosslinkers which is the main challenge for designing hydrogels with the desired physicochemical properties [8, 21].

Nanoparticles are well-known as very efficient cross-linking agents because of their high surface activity and large number of functional groups [4, 9, 22, 23]. CDs, spherical nanoparticles with the size smaller than 10 nm,

have attracted great interest due to their biocompatibility, low toxicity, antibacterial activity, excellent water solubility, and easy synthesis methods using accessible materials. CDs which have intrinsic functional groups such as  $-\text{COOH}$ ,  $-\text{OH}$ , and  $-\text{NH}_2$ , can be further functionalized to enhance their solubility, antibacterial performance, and crosslinking potential [13, 24–26].

Chengjian Mou et al. created an injectable self-healing hydrogel using CDs as crosslinkers in  $\epsilon$ -polylysine that improved wound-healing properties and broad-spectrum antibacterial activity [27]. Based on detecting the wound state indicators, Xin Ting Zheng et al. doped CDs in hydrogel's matrix as a cross-linker and colourimetric detector [28].

In addition, CDs could inherit specific properties from their natural sources and also have the potential to be doped with other chemicals or agents and ions such as calcium [25, 29]. Calcium ions play a crucial role in improving the hemostatic effectiveness of hydrogels by actively participating in the blood-clotting cascade [30, 31]. In this study, the calcium-doped CDs are synthesized from Coriander leaves as natural sources with antibacterial activity [32–34].

Preventing the growth of bacterial and microbial infections which could result in delaying the wound healing process is a crucial aspect that should be taken into account while managing wound healing [3, 35]. Every chemical antibacterial agent has distinct side effects, both systemically and locally which could result in delayed wound healing by inducing cytotoxicity and stimulating the acute inflammatory reaction [36, 37]. In contrast, herbal medicines play a crucial role in reducing inflammation, facilitating disinfection, and creating a favourable environment that supports the natural healing process [3, 38].

The plant known as *Bistorta officinalis* Delalbre, belonging to the Polygonaceae family, has been used historically in Asia and Europe for its topical anti-inflammatory and blood clotting properties [39, 40]. Several studies have investigated the ethnopharmacological properties of bistort such as hemostasis [41–44], anti-inflammatory [45] antibacterial effect [46] antivirulence [47], and even anti-cancer [48]. Prior investigations into the phytochemical makeup of the underground components of bistort have unveiled the presence of phenolic acid derivatives, triterpenoids, coumarins, steroids, flavan-3-ols, and galloyl glucose [39, 45, 46, 49].

This study presents the development of a novel biomaterial-based nanohydrogel film that incorporates green-synthesized CDs as crosslinking agents and BEX for enhanced antibacterial and blood-clotting performance. By leveraging the unique properties of natural biomaterials and nanotechnology, this approach seeks to address the limitations of conventional wound-healing strategies,

offering a biocompatible and cost-effective solution for advanced wound management (Fig. 1).

## Results and discussion

### Synthesis and characterization of cds

The hydrothermal method, a quick, easy, and economical way to synthesize nanoparticles, was used to synthesize the CDs by precursors from the extract solution of coriander leaves and  $\text{CaCl}_2$ .

The dynamic light scattering (DLS) analysis result (Fig. 2a, b) illustrates how CDs are monodispersed, with hydrodynamic particle sizes of about 6 nm and zeta potentials of around  $-10.8$  mV. The SEM and TEM images demonstrated that the spherical CDs, with a particle size of about 6 nm, were effectively synthesized (Fig. 2c, d).

The surface elemental analysis of CDs was performed using energy-dispersive X-ray spectroscopy (EDS) with elemental mapping (Fig. 3). It demonstrates that the O, C, N, Ca, Mg, K, Cl, and Na make up the majority of the CDs' surface. The most important minerals in the coriander are O, C, N, Ca, Mg, K, and Na; these elements are transferred to the CD's structure following the synthesizing process and CDs have been able to inherit the characteristics of the original source very well [32, 33]. In addition, since the  $\text{CaCl}_2$  is used as a precursor in CDs, the Cl is also doped to the structure as well; This result shows that the Ca successfully doped to the structure.

To determine the chemical components, functional groups, and surface composition of the extracted coriander leaves and synthesized CDs, Fourier transform infrared (FT-IR) spectra were employed (Fig. 3a). The results show the presence of a variety of functional groups as is common in plant extracts.

Both spectra have large peaks around  $3423\text{ cm}^{-1}$  and  $3436\text{ cm}^{-1}$  (synthesized carbon dots); they are indicative of the existence of O-H and N-H stretching vibrations, which are frequently found in amines, phenols, and alcohols. The  $1622\text{ cm}^{-1}$  and  $1051\text{ cm}^{-1}$  peaks in the coriander leaves that are moved in the synthesized carbon dots to  $1635\text{ cm}^{-1}$  and  $1073\text{ cm}^{-1}$  respectively (potential C-O and C=O stretching), indicating that these groups play a role in CD synthesis.

The synthesized carbon dots exhibit peaks at  $1145$ ,  $1452$ , and  $1565\text{ cm}^{-1}$ , indicating the presence of additional peaks not clearly seen in the coriander leaf spectrum that indicate the emergence of new bands. While the FTIR signal from the coriander leaves, at  $1397\text{ cm}^{-1}$ , reveals C-H bonds, the synthesized carbon dots exhibit additional peaks at  $1386\text{ cm}^{-1}$ , suggesting changes or new functional groups due to the synthesis process. In coriander leaves, the Mg-N stretching in chlorophyll has a pronounced peak around  $500\text{--}700\text{ cm}^{-1}$ ; in synthesized carbon dots, this peak is nearly absent, indicating that the structure of the chlorophyll has changed after the synthesized process. This outcome aligns with the Excitation and Emission result (Fig. 4), which shows that following

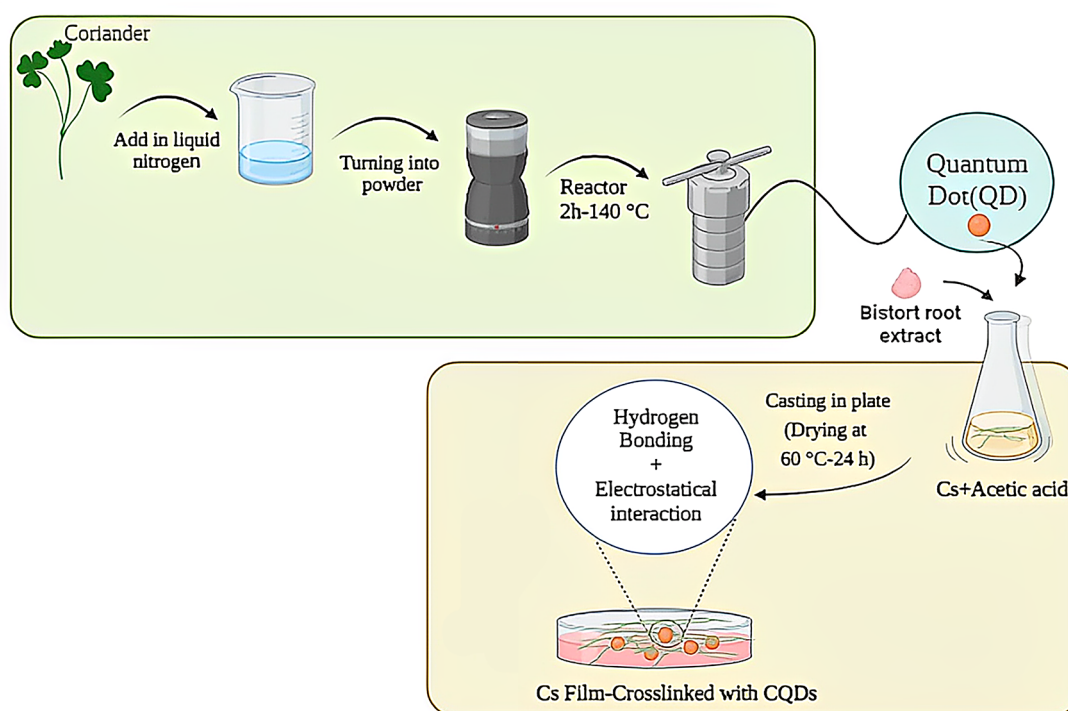


**Fig. 1** A schematic illustration of the development of a hydrogel film by crosslinking process between CS and CDs, along with the integration of BEX

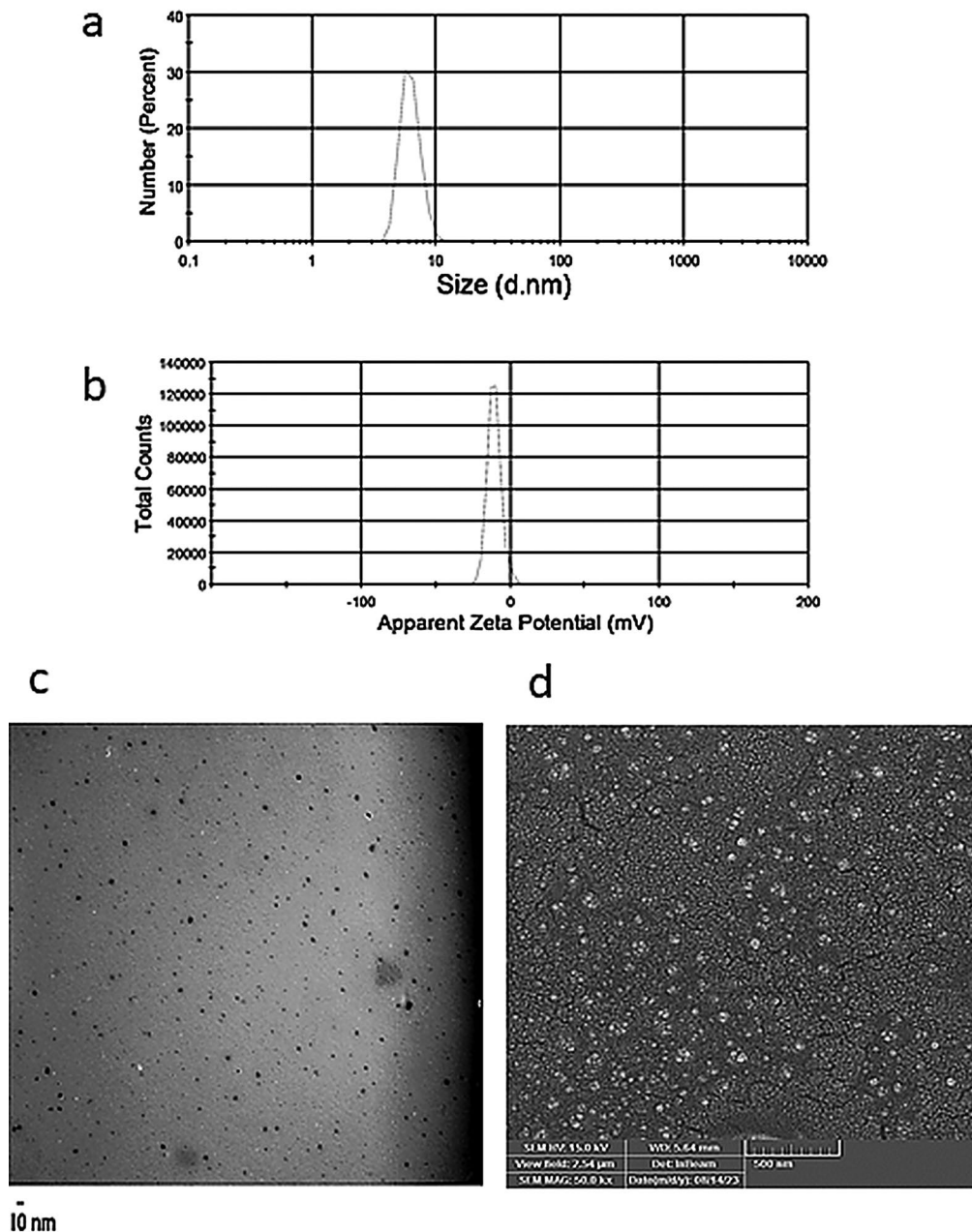


**Fig. 2** DLS shows that (a) particle size is monodisperse and around 6 nm. (b) The Zeta potential of the nanoparticle is negative and around  $-10.8$  mV. (c) TEM and (d) SEM images of synthesized CDs show spherical morphology with good dispersion and homogeneous particles

the CD synthesizing procedure, the coriander leaves' red chlorophyll emission changed to blue under the UV lamp. Overall, the comparison of the FTIR spectra shows that some of the original functional groups from the coriander leaves have been maintained in the synthesized carbon dots from the leaves and that the synthesis process has either introduced new bonds or made them more apparent.

According to the XRD results (Fig. 3d), the examined nanoparticle has an almost amorphous overall structure. The broad peak is around  $25^\circ$ , which is equivalent to a

$0.34$  nm lattice spacing; such a hump has been frequently seen in amorphous carbon XRD patterns. The XRD pattern that was observed also roughly matched the standard diffraction pattern [Ref. Code 96-201-0755] [50].

According to Uv-vis absorption (Fig. 4), the peaks that have been observed within the range of  $240$ – $300$  nm and  $300$ – $390$  nm are associated with  $\pi \rightarrow \pi^*$  and  $n \rightarrow \pi^*$  transitions of C=C, C–C, and C=O [51]. The peak between  $300$  and  $390$  nm altered in the CD-dCDs, indicating that the synthesis was successful. This finding is consistent with the FTIR data, which indicate that the predominant

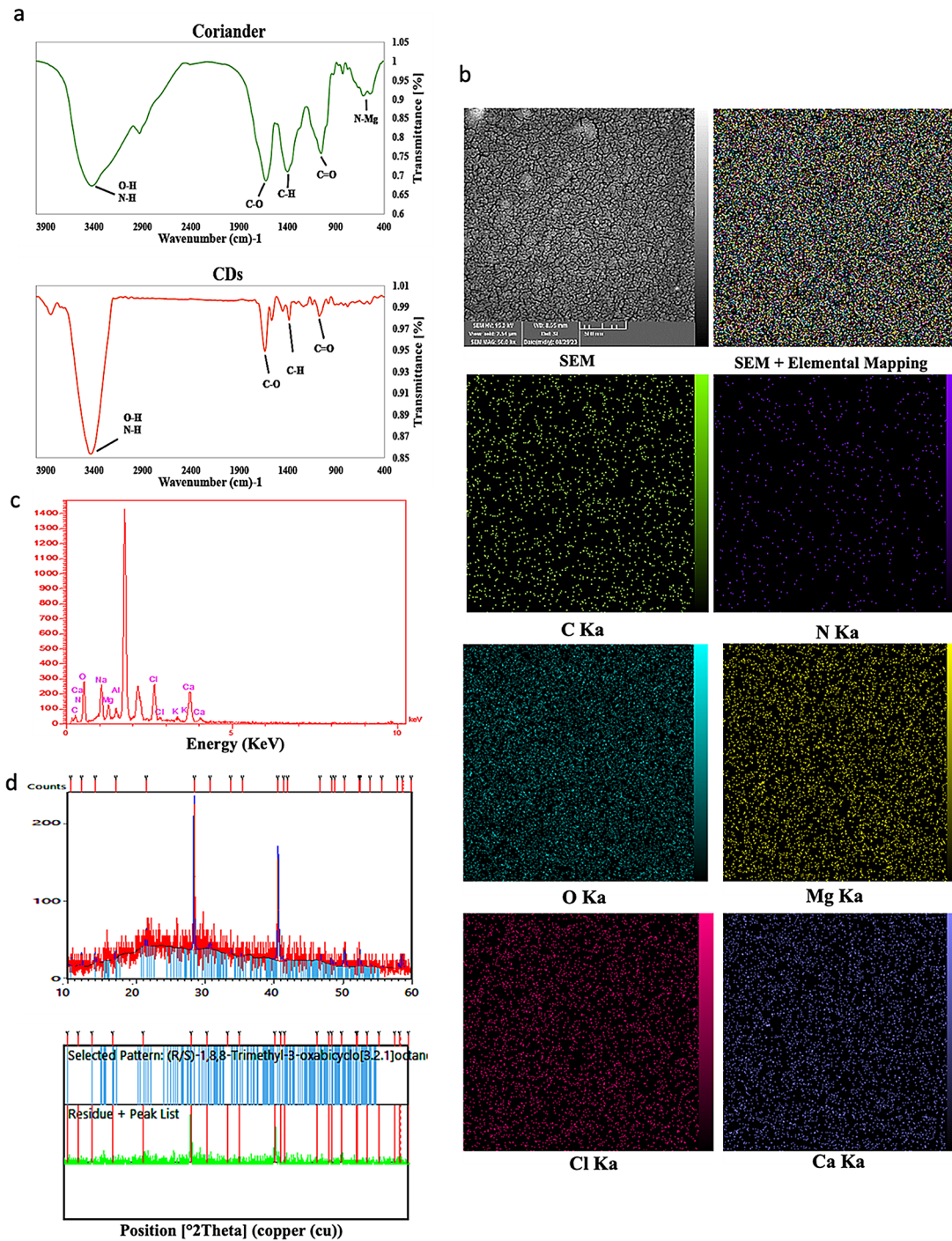


**Fig. 3** (a) FT-IR spectrum of CDs. (b) CD elemental mapping images showing the distribution and presence of the generally distributed elements C, O, N, Ca, Mg, Cl, and Ca. (c) EDS spectra for CDs. (d) XRD diffraction pattern of CDs

stretching involved in the synthesis of carbon nanoparticles was in the functional bands of C=O and C-O.

The CDs have a maximum excitation of around 360 nm, according to the PL spectra (Fig. 4), and the emission peak is red-shifted to around 500 nm when the excitation wavelength is raised from 320 nm to 400 nm. In the meanwhile, the peak emission occurs at 480 nm is inside

the visible blue light spectrum. As a result, we see the quantity of blue emission from CD nanoparticles under the gel doc (Fig. 4e); whereas, the Corriador extract's red emission under gel doc is caused by the presence of chlorophyll which this finding indicates that the synthesis of carbon dots was successful and the raw Corriador extract's structure changed during the synthesis process.

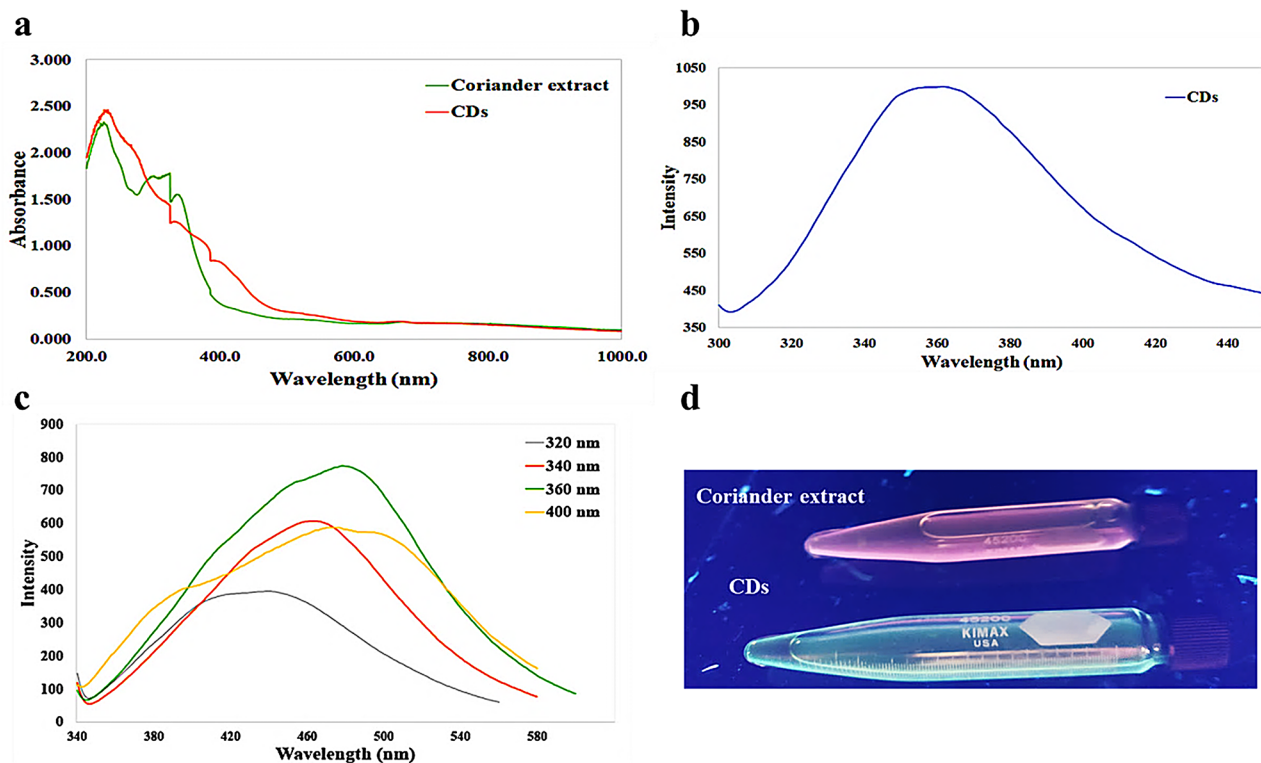


**Fig. 4** (a) Uv – vis results in different wavelengths (from 300 to 1000) for Coriander leaf extracts and CDs. (b) Excitation of the CDs. (c) Emission spectra of CDs at different excitation wavelengths. (d) emission of Coriander leaf extracts and CD samples under the gel doc

The distribution of surface states of nanoparticles with varying energy levels is linked to the excitation-dependent emission performance of CDs whereas CDs emit blue light. The quantum yield was determined to be 15% based on the research presented by Williams et al. [52] and the excitation and emission of CD nanoparticles.

#### Synthesis and characterization of the hydrogel film

A variety of CD concentrations (5%, 10%, and 15% of the CS weight) were used as a crosslinking agent in this study, and a range of BEX concentrations (10%, 20%, and 40% of the CS weight) were added to the CS matrix via the simple casting method. When the various concentrations of doped carbon dots were compared, the CDs 10% made good cross-link in CS, the optimal balance between strength and ductility (Fig. 5), and resulted in a stable structure with maximum uptake of BEX. In the higher concentration of CDs, the uptake of BEX decreased and the structure was so rough with low flexibility which is consistent with the results of the SEM (Fig. 6) and force-extension curve (Fig. 5). The maximum concentration of uptake BEX was 40% which in the higher concentrations than 40% the amount of sediment showed after the synthesizing process indicates the limitation of BEX uptake, so the final film produced based on CDs 10% and BEX 40%. Because of its plasticizing and bioactive properties,

glycerol was also used in the formation of the nanohydrogel film.

The force-extension curves for the CS film, CS/CD 5%, CS/CD 10%, and CS/CD 15% are displayed in Fig. 5. Each sample has an initial linear section that displays a forced rise that is proportionate to extension, illustrating elastic behaviour. The yield point and Ultimate Tensile Strength (UTS) in the blank film are lower than in crosslinked films, and it shows some plastic deformation before breaking, suggesting moderate ductility. CS films that have CDs incorporated as crosslinkers exhibit a notable improvement in their mechanical features, including yield strength, stiffness, and UTS. Strength and ductility have a trade-off; greater CD concentrations make films stronger but may also make them less flexible. The 10% CD concentration seems to give an excellent balance between strength and ductility, making it perhaps the best choice for applications requiring both features. Over-crosslinking (e.g., 15% CDs) might lead to increased fragility, which might not be desired for all applications.

The SEM pictures of the blank, CS/CD 10%, and final film are shown in Fig. 6. According to the SEM pictures, the surface morphology of every film is consistent; yet, the surface morphology of the nanocomposite was somewhat altered to a rougher state by adding CDs and BEX which this result is consistent with the tensile result.

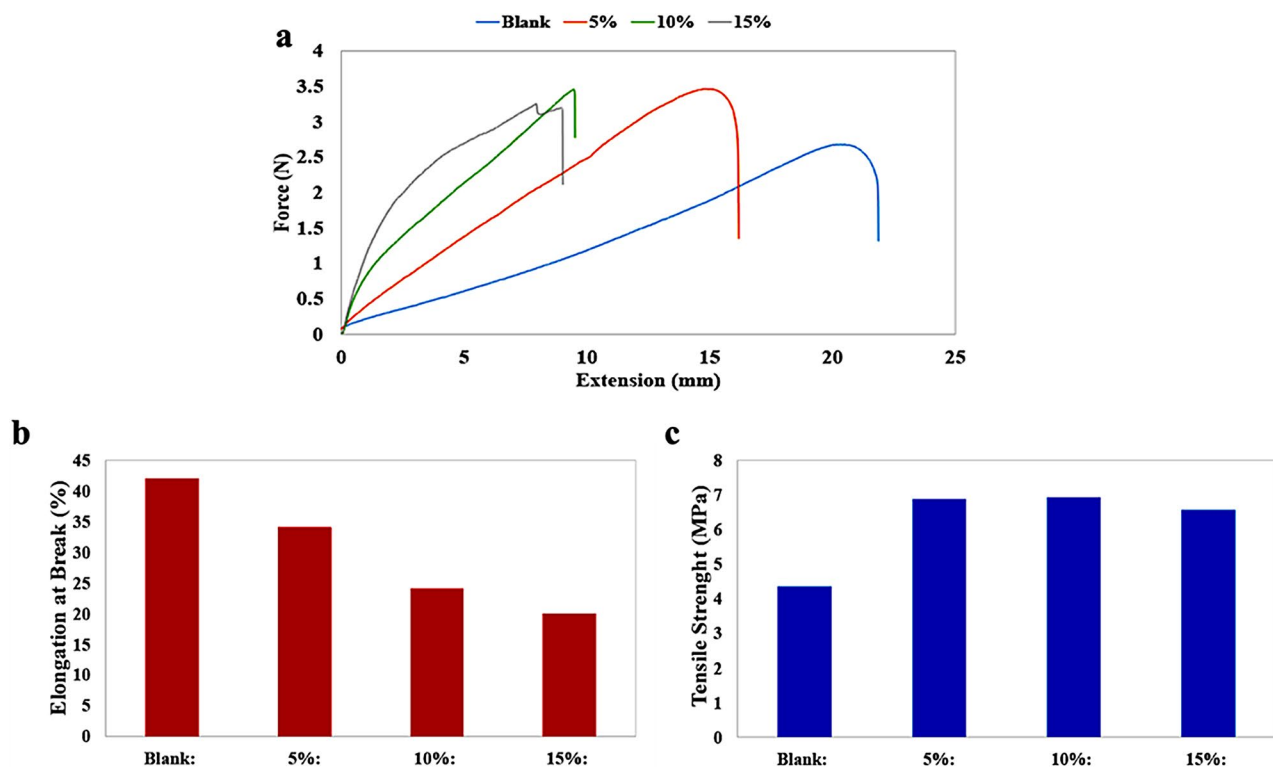


**Fig. 5** (a) Stress, (b) elongation at break, and (c) tensile strength of the CS, CS/CD with different CDs

The UV-visible absorbance result (Fig. 6b) shows absorbance across the entire unvisible spectrum by the blank film. After cross-linking the film by CDs, an absorption peak around 280 nm with a peak around 320 nm, potentially from  $n-\pi^*$  transitions in aromatic compounds (likely from carbon dots) [25, 51, 53]. The final film absorbance is similar to the CS/CD 10% around 280–320 nm; however, there is an additional peak around 500 nm which aligns with the previous studies and the UV-visible absorbance result of the Bistorta family [54]. All things considered, this outcome demonstrates the final film's successful synthesis.

The FT-IR spectra of CS, CS & CDs 10%, and the final film are considered to have demonstrated the effective construction of the nanohydrogel film and the comprehension of the chemical interactions and alterations in the film structure (Fig. 6).

All three films show prominent peaks in the regions around  $3400\text{ cm}^{-1}$ ,  $1600\text{ cm}^{-1}$ ,  $1400\text{ cm}^{-1}$ , and  $600\text{ cm}^{-1}$ . These peaks typically indicate the presence of O-H and N-H stretching vibrations, C=O stretching vibrations, C-O stretching vibrations in the carboxylate group stretching vibrations, and N-H stretching vibrations in primary amine groups ( $\text{NH}_2$ ) in out-of-plane bending vibrations, respectively. CS's hydroxyl functional and amine groups can form hydrogen bonds and electrostatic

interactions, respectively, with the carboxylate functional groups in the CDs [55].

The  $1100\text{--}1000\text{ cm}^{-1}$  region is indicative of C-O stretching vibrations in blank film, characteristic of polysaccharides which is almost constant in CD 10% and final film.

Unique peaks in the final film at  $1078\text{ cm}^{-1}$  and  $978\text{ cm}^{-1}$ , and variations in peak intensities even in the common peaks, suggest different chemical interactions or additional functional groups present in the final film compared to the other samples which these differences reflect the structural modifications and new interactions introduced by the CDs or BEX in the CS matrix.

The films' swelling behavior in PBS (pH 7.4) at  $37\text{ }^\circ\text{C}$  is shown in Fig. 6c. The produced nanohydrogel films' capacity to absorb wound moisture is directly correlated with the swelling findings. It was demonstrated that when immersion time increased, the swelling ratio increased considerably. By adding CDs and BEX to the CS polymeric matrix, the swelling ratio is reduced which may be according to the crosslinking of the CS that resulted in increasing the hydrogel network's hardness [56]. Moreover, incorporating BEX could make the film more robust and decrease the swelling rate. The polyphenols, tannins, and other bioactive substances in BEX can create additional crosslinks within the film, improving its

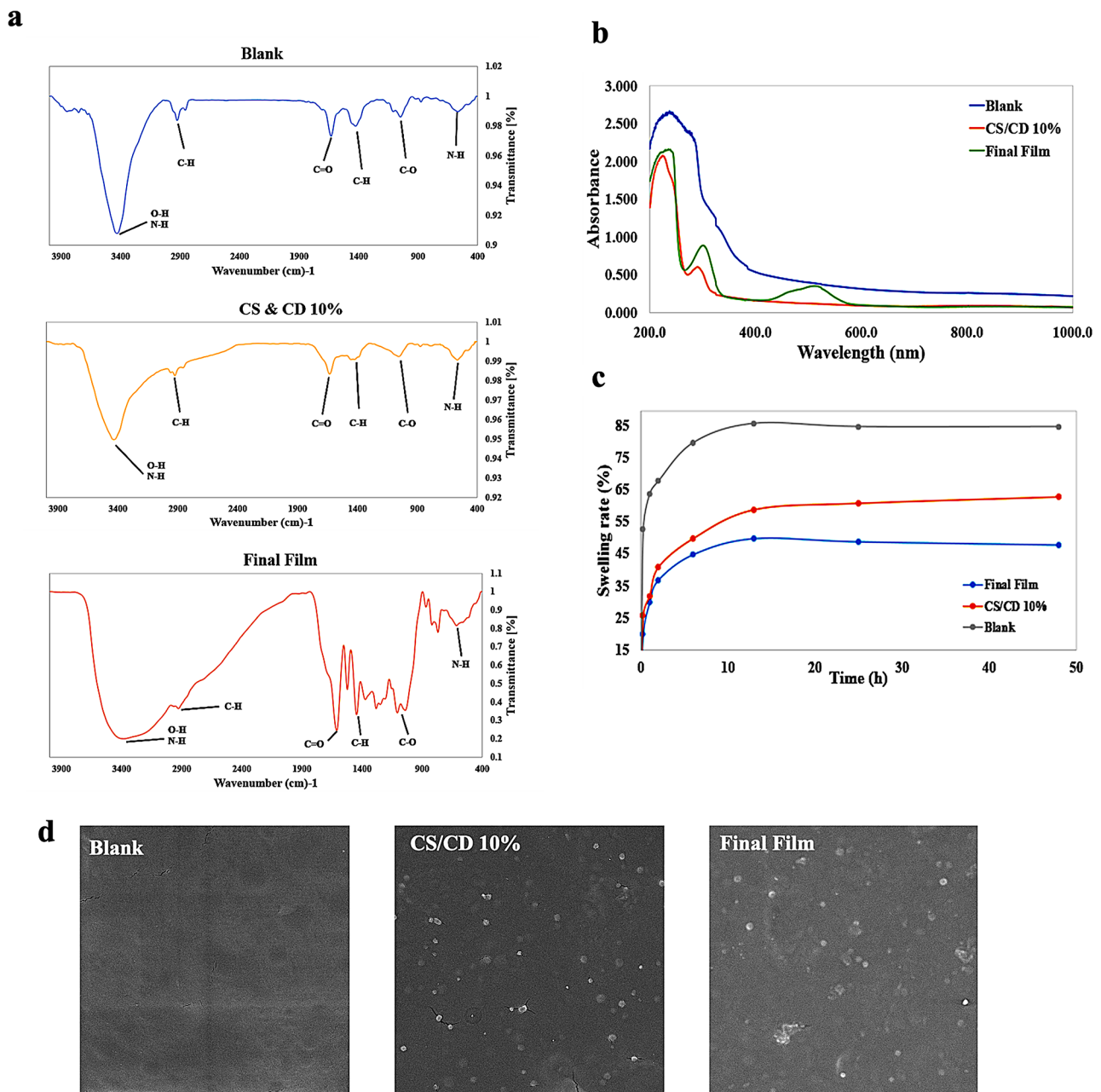


**Fig. 6** (a) FTIR results for Cs film (blank), CS/CD 10%, and final film, (b) Uv–vis results in different wavelengths (from 200 to 1000) for blank, CS/CD 10%, and final film, (c) The swelling ratio in PBS (pH 7.4) at 37 °C for the CS, CS/CD 10%, and final film, and (d) SEM result of blank, CS/CD 10%, and final film

overall stability [45, 46, 49] which is consistent with the SEM results (Fig. 6d).

The blood clotting capacity is an essential feature of biomaterials-based wound dressings. Figure 7 displays the blood clotting study's findings the results show that adding 10% of CD in films has improved its blood clotting capacity. These results could be due to the inheritance of calcium from the coriander as well as additionally calcium doped into the CDs' structure (32, 33). After incorporating BEX, the blood clotting ability of the CS film

significantly increased and matched the effectiveness of commercial gauze and other studies [18, 27].

The hemolytic effects were respectively increased by the hemolysis rate to 8.96% with crosslinking the film with CDs in the formulation process and the increase continues with the addition of BEX to 18.22%. The majority of the hemolysis often occurred after the extract was added; however, the final film hemolysis was less than 20% (Fig. 7). Additionally, the optical picture in Fig. 7 showed the treated films' supernatant containing red blood cells which is insignificant when compared to the

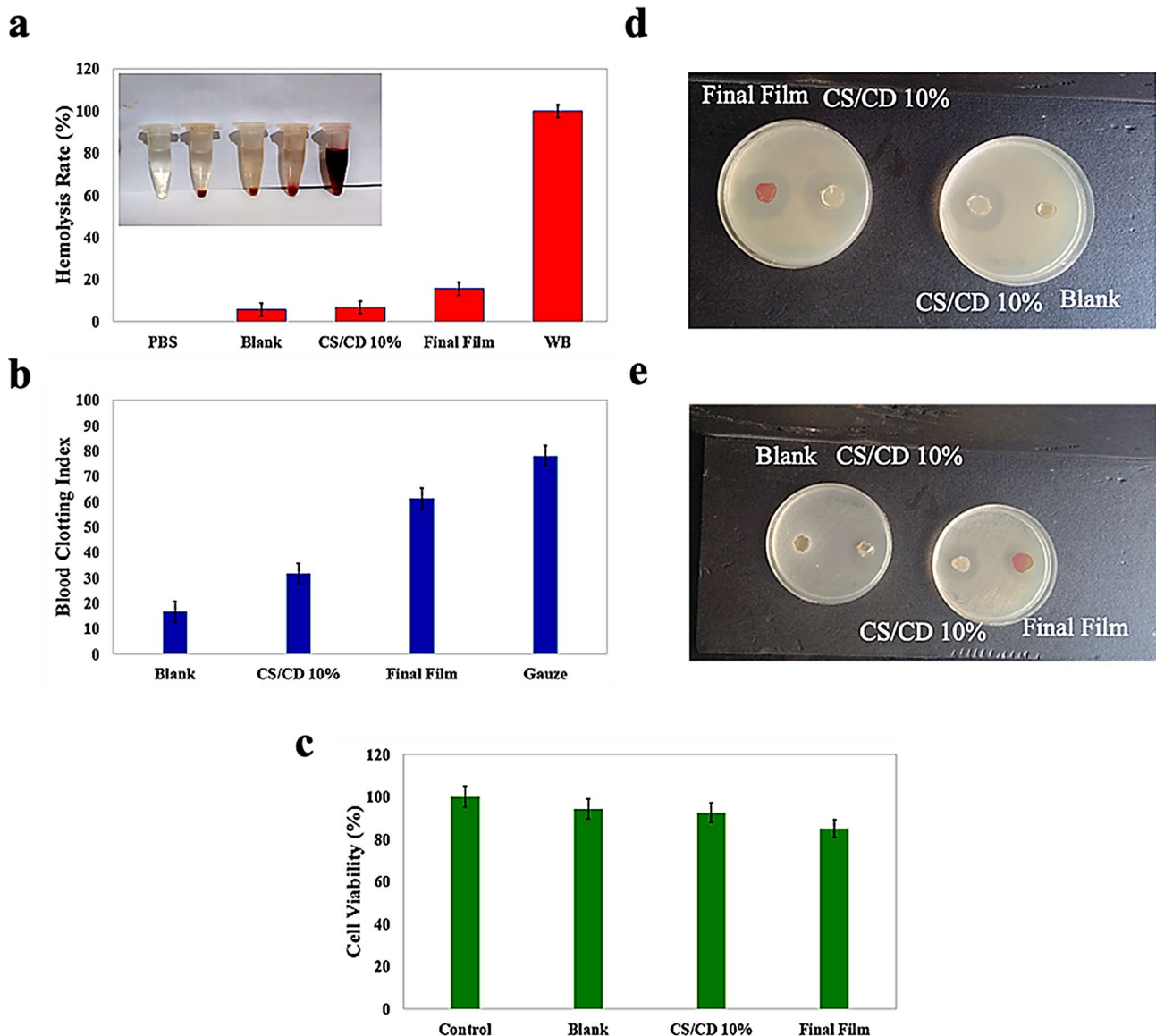


**Fig. 7** (a) Hemolysis rate, (b) Blood clotting index (c) Cell viability of Blank, CS/CD 10%, and final films after incubation with human blood and human red blood cells (erythrocytes). Images of the antibacterial inhibition zones for CS, CS/CD 10%, and final film against (d) *E. coli* and (e) *S. aureus*

negative control (PBS). With its exceptional blood clotting index, the synthesized film is the preferred option for use as a wound application.

The cytotoxicity of the CS, CS/CD 10%, and final film on HFF-1 cell lines was tested using the MTT method (Fig. 7) and even after 48 h, nearly 80% of the samples' cell viability was maintained.

The results indicate that the cytotoxicity of hydrogels was slightly enhanced with treatment time and the amount of CDs and BEX in the nanohydrogel. So there is a direct correlation between the concentration of these substances employed in nanohydrogel films and the toxicity of the films. This good result and low toxicity are due to the use of biological precursors in film synthesis

[7, 39]. Based on the findings, produced films could offer an effective and safe basis for wound dressing.

The antibacterial activity of the produced films was investigated using disc diffusion techniques against microorganisms *S. aureus* and *E. coli* (the most popular gram-positive and gram-negative bacteria) in order to explain their antibacterial performance [57, 58] (Fig. 7).

Figure 7 displays that after cross-linking with CDs and adding the BEX into the structure, the antibacterial property of the film has significantly increased (especially against *E. coli*) compared to the blank CS film, which is a sign of the antibacterial property of the precursors used and is consistent with the previous studies [34, 39].

## Conclusion

In this study, a biomaterial-based nanohydrogel film composed of CS polymer cross-linked with CDs and included BEX as an antibacterial and blood clotting agent was effectively developed. Calcium-doped CDs were synthesized from Coriander leaves using the hydrothermal method, offering a quick and easy method for producing nanoparticles on large scales that could potentially utilized in wound dressings. Comprehensive analysis and characterization of the synthesized CDs conclusively demonstrated their monodispersed spherical morphology (~6 nm), negative surface charge (-10 mV), and presence of active functional groups such as C-O and C=O. These properties of synthesized CDs enabled effective cross-linking within the CS matrix through chemical bonding and electrostatic interactions, significantly enhancing the mechanical strength and stability of the hydrogel film (improving stress and elongation at the break by approximately 3 MPa and 20%, respectively).

The successful fabrication and structural properties of the developed hydrogel film were investigated using various analytical techniques, including FT-IR, UV-Vis, swelling rate measurements, stress and elongation, and SEM. The synthesized hydrogel film exhibited the desired blood clotting (~60%), low cytotoxicity against human skin fibroblast (HFF-1) cell lines (over 80% cell viability in the highest concentration), and notable antibacterial activity against gram-positive and gram-negative bacterial strains, making it a promising candidate for wound healing applications. Furthermore, the presence of calcium-doped CDs, alongside BEX, also played a role in enhancing blood coagulation and antibacterial activity.

This study highlights the potential of biomaterial-based nanohydrogel films for wound dressing applications by promoting blood clotting and preventing microbial infections. The incorporation of BEX also offers potential for future research in biomaterial-based hydrogels and potential synergies with other blood-clotting agents. However, variability in BEX composition due to differences in plant sources and extraction methods may affect hydrogel reproducibility, necessitating further standardization. Future research could prioritize in vivo evaluations and direct comparisons with commercial wound dressings to validate the hydrogel's clinical applicability and effectiveness.

## Material and method

### Statistical analysis

All tests were conducted in triplicate, with results from one representative data set being reported. The data were expressed as mean ± standard deviation (SD). Statistical differences in the examined parameters among the samples were evaluated using ANOVA followed by the Tukey-Kramer post-hoc test, performed with Excel and

Prism 9 software (GraphPad Software Inc.). XRD analysis was carried out using High-score software, while FTIR spectra were processed with IRpal software. P values less than 0.05 were considered significant.

### Material

Dulbeccom-modified Eagle medium (DMEM), trypsin-EDTA, penicillin, streptomycin, and fetal bovine serum (FBS) were purchased from Gibco BRL Life Technologies. The dialysis bags (MWCO = 1 kDa) and 3-(4,5-dimethylthiazol-2-yl)-2,5-diphenyl tetrazolium bromide (MTT) were purchased from Sigma-Aldrich Company. Calcium chloride (CaCl<sub>2</sub>), CS (99.5%, medium molecular weight), Glycerol (99.5%), and all other chemicals were procured from Merck Co. Fresh coriander was obtained from a reputable store and Fresh Bistorta powder was obtained from Giyah Kala Company.

### Method

#### Nanoparticle synthesis

The hydrothermal technique was used to create the CDs (Scheme 1). In simple terms, coriander leaves were cleaned to get rid of impurities, then cut into tiny pieces and ground into a powder using an electric grain grinder. Next, 5 g of obtained powder was combined with 100 ml of mixed deionized water and alcohol (50/50). After 30 min of sonication, the combined solution was filtered and after adding 6 mg of CaCl<sub>2</sub> to the mixture, the mixture was put into the reactor and heated to 140 °C for four hours. To get the pure powder of CDs, the product was filtered, centrifuged for 15 min at 9000 rpm, and dialyzed. Finally, CDs powder was obtained by freeze-drying the sample.

#### Characterization of cds

CDs were analyzed by dynamic light scattering (DLS, Zetasizer Nano ZS90, Malvern Instruments, Malvern, UK) and transmission electron microscopy (Hitachi 700, Hitachi High Technologies America, Inc., Pleasanton, CA, Twinsburg, OH, USA) to assess their shape, size, and zeta potential.

X-ray diffraction (XRD) using Cu K $\alpha$  radiation on a Rigaku D/max 2500 system was used to investigate the crystallinity of carbon dots. Fluorescence emission spectra were recorded on a NOVA fiber-coupled spectrometer. The absorption behavior of the CDs was recorded by the UV-vis double beam PC 1650 UV-Vis (SHIMADZU, Kyoto, Japan) spectrometer. With the TENSOR27-Brucker Spectrometer, Fourier transform infrared (FT-IR) spectroscopy, the structure and content of CDs were examined. CDs were analyzed using FESEM and EDS (MIRA3TESCAN-XMU) to examine their shape and surface elemental composition.

Williams et al.'s relative technique was used to measure the quantum yields [52]:

$$Q_x = Q_s \frac{F_s}{F_x} \frac{A_x}{A_s} \frac{\eta_s^2}{\eta_x^2} \quad (1)$$

where Q is the quantum yield, F is the integral of the fluorescence emission scan, A is the absorbance,  $\eta$  is the index of refraction of the solvent, x indicates the type of sample to be analyzed, and s denotes the reference material. Since the manufactured CDs had identical excitation and emission wavelengths, quinine sulfate (fluorescence quantum yield of 0.54) was used as the standard fluorescent agent. To get rid of errors from internal reflection and reabsorption, the samples were diluted.

#### Preparation of CS/CD/BEX nanohydrogel films

To prepare nano hydrogel films, a certain amount of CS powder (1.000 g) dissolved in 0.1% (w/v) acetic acid solution to create a homogeneous 1% (w/v) CS solution and stirred for one hour at room temperature.

In order to obtain 5%, 10%, and 15% CD solutions with a weight ratio of CDs to CS, specific quantities of CDs (0.050, 0.100, and 0.150 g) were dissolved in 20 ml of distilled water and added in separate containers to the previous CS solution. Afterwards, BEX (0.1, 0.2, and 0.4 g) were separately added to the solution and stirred until dissolving, followed by adding glycerol (0.5% w/v), as a plasticizer, stirred for 4 h at 45 °C to prepare the film with 10%, 20%, and 40% of BEX (weight ratio of BEX to CS). The resulting clear and homogenous paste (25 mL) was poured onto a 10-cm-diameter polystyrene plate and allowed it to dry for 24 h at 60 °C.

#### Swelling study

A physiological temperature (37 °C) solution of phosphate-buffered saline (PBS, pH 7.4) was used to perform an in-vitro swelling evaluation. the hydrogel film samples (CS, CS/CD, and final film) were immersed in 20 ml of the buffered solution and then weighted ( $W_i$ ).

Samples were taken out at specified intervals to calculate the swelling ratio. After removing surface water with filter paper, the samples were weighted ( $W_t$ ). The swelling ratio was obtained by applying the subsequent formula (Eq. 1):

$$\text{Swelling ratio} = \frac{W_t - W_i}{W_i} \quad (2)$$

#### Cytotoxicity assays

In 25  $cm^2$  culture flasks with 5% CO<sub>2</sub>, the HFF-1 cells were incubated in the full Dulbeccom modified Eagle medium (DMEM, high glucose formulation; 10% (v/v) fetal bovine serum and 1% (v/v) penicillin-streptomycin)

until at least 70% confluency. Then the cytotoxicity of the developed films was assessed on HFF-1 cells, utilizing an established MTT test.

#### Blood clotting

The performance of the blood clotting test is demonstrated by reported procedures [59]. First, all of the 10 mm-diameter sliced films were inserted into the 12 wellplates, and they were kept warm for 15 min at 37 °C in an incubator. Sodium citrate was used as an anticoagulant to stabilize the fresh human blood. After that, 200  $\mu$ L of stabilized blood was progressively dripped onto the films. In this instance, the gauze-wearing controls received no sample. Subsequently, 40  $\mu$ L of 0.2 M CaCl<sub>2</sub> solution was added to the blood samples to start the blood-clotting process.

The clotting trapped the red blood cells after they were incubated for 15 min at 37 °C. Then, 6 mL of deionized water was added to each well to hemolyze the blood cells. 2 mL of the media were removed and centrifuged for 2 min at 1500 rpm after 2 min of moderate shaking. A BioTech ELISA reader was used to measure the supernatant's absorbance in water at 540 nm. Equation 2 was utilized to calculate the blood clotting index (BCI) for diverse samples.

$$BCI = \frac{OD_{sample}}{OD_{control}} \quad (3)$$

Blood absorbances with and without samples were denoted by the terms  $OD_{sample}$  and  $OD_{control}$  respectively.

#### Hemolysis rate assay

The hemolysis test was carried out in compliance with earlier research [59]. In the beginning, the stable human fresh blood supernatant (plasma) was collected by centrifuging. To get rid of any lysed hemoglobin, the pellets—which are human red blood cells—were washed three times with PBS (pH 7.4).

After dilution ten times in PBS, the pellets were combined with 1 mL of PBS containing CS, CS with 10% CD, and final film and incubated for sixty minutes at 37 °C. In the negative control, 0% hemolysis was achieved using PBS solution, whereas 100% hemolysis was obtained in the positive control using double-distilled water. After being incubated, the samples were transferred to the 96-well plates and centrifuged for 10 min at 3500 rpm. Utilizing a spectrophotometer adjusted to 545 nm, the absorbance of the supernatant was determined. Equation 3 was used to compute the hemolysis rate as a percentage.

$$\text{Hemolysis Rate (\%)} = \frac{Abs_{sample} - Abs_{PBS}}{Abs_{water} - Abs_{PBS}} * 100 \quad (4)$$

### Antimicrobial activity

The agar disc diffusion technique was used to measure the antibacterial performance.

[60]. The developed nanohydrogel films were tested against gram-positive and gram-negative pathogens to look into their antibacterial properties; the findings are shown in Fig. 7. The bacterial strains were treated on the agar plate surface following their adjustment to the 0.5 McFarland standard. Afterwards, sterile cutting of all films to an 8 mm diameter, they were placed on agar plates and incubated at 37 °C. The inhibitory zones were tested 18–24 h later.

### Abbreviations

BEX	Bistorta officinalis extraction
CDs	Carbon dots
CS	Chitosan
PBS	Phosphate buffer serum
BCI	Blood clotting index
MTT	3-(4,5-dimethylthiazol-2-yl)-2,5-diphenyltetrazolium bromide
DMEM	Dulbeccom-modified Eagle medium
FBS	Fetal bovine serum
DLS	The dynamic light scattering
TEM	Transmission electron microscopy
SEM	Scanning electron microscope

### Acknowledgements

Not applicable.

### Author contributions

Meysam Najafloo: ES and FG Hassan Tavakoli: ES and FG Ahmad Yari Khosroushahi: ES and FG.

### Funding

Not applicable.

### Data availability

No datasets were generated or analysed during the current study.

### Declarations

#### Ethics approval and consent to participate

Not applicable.

#### Consent for publication

Not applicable.

#### Competing interests

The authors declare no competing interests.

Received: 19 December 2024 / Accepted: 1 April 2025

Published online: 10 April 2025

### References

- Proksch E, Brandner JM, Jensen JM. The skin: an indispensable barrier. *Exp Dermatol*. 2008;17(12):1063–72.
- Sorg H, Tilkorn DJ, Hager S, Hauser J, Mirastschijski U. Skin wound healing: an update on the current knowledge and concepts. *Eur Surg Res*. 2017;58(1–2):81–94.
- Ansari M, Darvishi A. A review of the current state of natural biomaterials in wound healing applications. *Front Bioeng Biotechnol*. 2024;12:1309541.
- Mamidi N, Velasco Delgadillo RM, Barrera EV. Covalently functionalized carbon nano-onions integrated gelatin methacryloyl nanocomposite hydrogel containing  $\gamma$ -cyclodextrin as drug carrier for high-performance pH-triggered drug release. *Pharmaceuticals*. 2021;14(4):291.
- Monika P, Chandrababha MN, Rangarajan A, Waiker PV, Chidambara Murthy KN. Challenges in healing wound: role of complementary and alternative medicine. *Front Nutr*. 2022;8:791899.
- Mamidi N, Ijadi F, Norahan MH. Leveraging the recent advancements in GelMA scaffolds for bone tissue engineering: an assessment of challenges and opportunities. *Biomacromolecules*. 2023;25(4):2075–113.
- Cao H, Duan L, Zhang Y, Cao J, Zhang K. Current hydrogel advances in physicochemical and biological response-driven biomedical application diversity. *Signal Transduct Target Therapy*. 2021;6(1):426.
- Pellá MC, Lima-Tenório MK, Tenório-Neto ET, Guilherme MR, Muniz EC, Rubira AF. Chitosan-based hydrogels: from Preparation to biomedical applications. *Carbohydr Polym*. 2018;196:233–45.
- Mamidi N, Delgadillo RMV. Design, fabrication and drug release potential of dual stimuli-responsive composite hydrogel nanoparticle interfaces. *Colloids Surf B*. 2021;204:111819.
- Mamidi N, De Silva FF, Vacas AB, Gutiérrez Gómez JA, Montes Goo NY, Mendoza DR, et al. Multifaceted hydrogel scaffolds: bridging the gap between biomedical needs and environmental sustainability. *Adv Healthc Mater*. 2024;13(27):2401195.
- Mamidi N, Poellmann M, Javius-Jones K, Nam K, Hong S. Innovative hydrogel-based delivery systems for immunotherapy: A review of pre-clinical progress. *Nano Res*. 2024;17(10):9031–43.
- Mamidi N, Otero JFF. Sustainable innovations in biomedical materials: A review of eco-friendly synthesis approaches. *Global Translational Med*. 2024;3(4):4698.
- Mamidi N, Delgadillo RMV, González-Ortiz A. Engineering of carbon nano-onion bioconjugates for biomedical applications. *Mater Sci Engineering: C*. 2021;120:111698.
- Mamidi N, Delgadillo RM. New Zein protein composites with high performance in phosphate removal, intrinsic antibacterial, and drug delivery capabilities. *ACS Appl Mater Interfaces*. 2024;16(29):37468–85.
- Farasati Far B, Naimi-Jamal MR, Jahanbakhshi M, Hadzadeh A, Dehghan S, Hadzadeh S. Enhanced antibacterial activity of porous chitosan-based hydrogels crosslinked with gelatin and metal ions. *Sci Rep*. 2024;14(1):7505.
- Nour-Eldin F. Chemical activation of Blood-clotting factors and thrombosis. *Nature*. 1967;214(5095):1362–3.
- Kumar MR, Muzzarelli RA, Muzzarelli C, Sashiwa H, Domb A. Chitosan chemistry and pharmaceutical perspectives. *Chem Rev*. 2004;104(12):6017–84.
- Guo S, Ren Y, Chang R, He Y, Zhang D, Guan F, et al. Injectable Self-Healing adhesive Chitosan hydrogel with antioxidative, antibacterial, and hemostatic activities for rapid hemostasis and skin wound healing. *ACS Appl Mater Interfaces*. 2022;14(30):34455–69.
- Guo B, Dong R, Liang Y, Li M. Haemostatic materials for wound healing applications. *Nat Reviews Chem*. 2021;5(11):773–91.
- Kaczmarek B, Nadolna K, Owczarek A. Chapter 6 - The physical and chemical properties of hydrogels based on natural polymers. In: Chen Y, editor. *Hydrogels based on natural polymers*. Elsevier; 2020. pp. 151–72.
- Kim S, Regitsky AU, Song J, Ilavsky J, McKinley GH, Holten-Andersen N. In situ mechanical reinforcement of polymer hydrogels via metal-coordinated crosslink mineralization. *Nat Commun*. 2021;12(1):667.
- Campea MA, Majcher MJ, Lofts A, Hoare T. A review of design and fabrication methods for nanoparticle network hydrogels for biomedical, environmental, and industrial applications. *Adv Funct Mater*. 2021;31(33):2102355.
- Liu Y, Song S, Liu S, Zhu X, Wang P. Application of nanomaterial in hydrogels related to wound healing. *J Nanomaterials*. 2022;2022(1):4656037.
- Dai C, Wan S, Li Z, Shi Y, Zhang S, Li Z. Switchable unidirectional emissions from hydrogel gratings with integrated carbon quantum Dots. *Nat Commun*. 2024;15(1):845.
- Najafloo M, Shahgolzari M, Bani F, Khosroushahi AY. Green synthesis of near-infrared copper-doped carbon Dots from alcea for cancer photothermal therapy. *ACS Omega*. 2022;7(38):34573–82.
- Mamidi N, Delgadillo RMV, Barrera EV, Ramakrishna S, Annabi N. Carbonaceous nanomaterials incorporated biomaterials: the present and future of the flourishing field. *Compos Part B: Eng*. 2022;243:110150.
- Mou C, Wang X, Teng J, Xie Z, Zheng M. Injectable self-healing hydrogel fabricated from antibacterial carbon Dots and  $\epsilon$ -polylysine for promoting bacteria-infected wound healing. *J Nanobiotechnol*. 2022;20(1):368.

28. Zheng XT, Zhong Y, Chu HE, Yu Y, Zhang Y, Chin JS, et al. Carbon Dot-Doped hydrogel sensor array for multiplexed colorimetric detection of wound healing. *ACS Appl Mater Interfaces*. 2023;15(14):17675–87.
29. Liu ML, Chen BB, Li CM, Huang CZ. Carbon Dots: synthesis, formation mechanism, fluorescence origin and sensing applications. *Green Chem*. 2019;21(3):449–71.
30. Singh S, Dodd J, Volkens P, Hethershaw E, Philippou H, Ivaskевич V, et al. Structure functional insights into calcium binding during the activation of coagulation factor XIII A. *Sci Rep*. 2019;9(1):11324.
31. Palta S, Saroa R, Palta A. Overview of the coagulation system. *Indian J Anaesth*. 2014;58(5):515–23.
32. Kerton M, Newbury HJ, Hand D, Pritchard J. Accumulation of calcium in the centre of leaves of coriander (*Coriandrum sativum* L.) is due to an uncoupling of water and ion transport. *J Exp Bot*. 2009;60(1):227–35.
33. AGRICULTURE USDO. Coriander (cilantro) leaves, raw: FoodData Central; 2018 [updated 2019. Available from: <https://fdc.nal.usda.gov/fdc-app.html#/food-details/169997/nutrients>
34. Kubo I, Fujita K-i, Kubo A, Nihei K-i, Ogura T. Antibacterial activity of coriander volatile compounds against *Salmonella choleraesuis*. *J Agric Food Chem*. 2004;52(11):3329–32.
35. Maver T, Maver U, Stana Kleinschek K, Smrke DM, Kreft S. A review of herbal medicines in wound healing. *Int J Dermatol*. 2015;54(7):740–51.
36. Punjataewakupt A, Napavichayanun S, Aramwit P. The downside of antimicrobial agents for wound healing. *Eur J Clin Microbiol Infect Dis*. 2019;38:39–54.
37. Knoop KA, McDonald KG, Kulkarni DH, Newberry RD. Antibiotics promote inflammation through the translocation of native commensal colonic bacteria. *Gut*. 2016;65(7):1100–9.
38. Xu Z, Dong M, Yin S, Dong J, Zhang M, Tian R, et al. Why traditional herbal medicine promotes wound healing: research from immune response, wound microbiome to controlled delivery. *Adv Drug Deliv Rev*. 2023;195:114764.
39. Pawłowska KA, Hałasa R, Dudek MK, Majdan M, Jankowska K, Granica S. Antibacterial and anti-inflammatory activity of Bistort (*Bistorta officinalis*) aqueous extract and its major components. Justification of the usage of the medicinal plant material as a traditional topical agent. *J Ethnopharmacol*. 2020;260:113077.
40. Manoharan KP, Benny TKH, Yang D. Cycloartane type triterpenoids from the rhizomes of polygonum Bistorta. *Phytochemistry*. 2005;66(19):2304–8.
41. Jarić S, Popović Z, Mačukanović-Jocić M, Djurdjević L, Mijatović M, Karadžić B, et al. An ethnobotanical study on the usage of wild medicinal herbs from Kopaonik mountain (Central Serbia). *J Ethnopharmacol*. 2007;111(1):160–75.
42. Jarić S, Kostić O, Mataruga Z, Pavlović D, Pavlović M, Mitrović M, et al. Traditional wound-healing plants used in the Balkan region (Southeast Europe). *J Ethnopharmacol*. 2018;211:311–28.
43. Kayani S, Ahmad M, Sultana S, Shinwari ZK, Zafar M, Yaseen G, et al. Ethnobotany of medicinal plants among the communities of alpine and Sub-alpine regions of Pakistan. *J Ethnopharmacol*. 2015;164:186–202.
44. Moiedie M, Vandoost J, Hajjar T, Mahdavi B. In vivo evaluation of polygonum Bistorta extract effect on blood coagulation factors. *Trends Phytochemical Res*. 2023;7(1):51–7.
45. Klimczak U, Woźniak M, Tomczyk M, Granica S. Chemical composition of edible aerial parts of meadow Bistort (*Persicaria Bistorta* (L.) Samp. Food Chem. 2017;230:281–90.
46. Intisar A, Zhang L, Luo H, Zhang R, Wu Z, Zhang W. Difference in essential oil composition of rhizome of polygonum Bistorta L. from different Asian regions and evaluation of its antibacterial activity. *J Essent Oil Bearing Plants*. 2012;15(6):964–71.
47. Jovanović M, Morić I, Nikolić B, Pavić A, Svirčev E, Šenerović L, et al. Anti-virulence potential and in vivo toxicity of persicaria maculosa and Bistorta officinalis extracts. *Molecules*. 2020;25(8):1811.
48. Intisar A, Zhang L, Luo H, Kiazolu JB, Zhang R, Zhang W. Anticancer constituents and cytotoxic activity of methanol-water extract of polygonum Bistorta L. *Afr J Tradit Complement Altern Med*. 2013;10(1):53–9.
49. Sun X-B, Zhao P-H, Xu Y-J, Sun L-M, Cao M-A, Yuan C-S. Chemical constituents from the roots of polygonum Bistorta. *Chem Nat Compd*. 2007;43:563–6.
50. Xu X, Ray R, Gu Y, Ploehn HJ, Gearheart L, Raker K, et al. Electrophoretic analysis and purification of fluorescent single-walled carbon nanotube fragments. *J Am Chem Soc*. 2004;126(40):12736–7.
51. Schmid FX. Biological macromolecules: UV-visible spectrophotometry. *e LS*. 2001.
52. Williams ATR, Winfield SA, Miller JN. Relative fluorescence quantum yields using a computer-controlled luminescence spectrometer. *Analyst*. 1983;108(1290):1067–71.
53. Noorkhajavi G, Abdian N, Najafloo M, Hefferon K, Yari-Khosroushahi A, Shahgolzari M. Synthesis of self-targeted carbon nanodot for efficient cancer cell imaging and therapy. *Inorg Chem Commun*. 2024;161:112027.
54. Ahmed F, Kabir H, Xiong H. Dual colorimetric sensor for Hg/Pb and an efficient catalyst based on silver nanoparticles mediating by the root extract of Bistorta amplexicaulis. *Front Chem*. 2020;8.
55. Versteeg HH, Heemskerk JW, Levi M, Reitsma PH. New fundamentals in hemostasis. *Physiol Rev*. 2013;93(1):327–58.
56. Bi L, Cao Z, Hu Y, Song Y, Yu L, Yang B, et al. Effects of different cross-linking conditions on the properties of genipin-cross-linked Chitosan/collagen scaffolds for cartilage tissue engineering. *J Mater Science: Mater Med*. 2011;22(1):51–62.
57. Jack RW, Tagg JR, Ray B. Bacteriocins of gram-positive bacteria. *Microbiol Rev*. 1995;59(2):171–200.
58. Pugsley A. The complete general secretory pathway in gram-negative bacteria. *Microbiol Rev*. 1993;57(1):50–108.
59. Smith SA, Choi SH, Davis-Harrison R, Huyck J, Boettcher J, Rienstra CM, et al. Polyphosphate exerts differential effects on blood clotting, depending on polymer size. *Blood J Am Soc Hematol*. 2010;116(20):4353–9.
60. Zaidan M, Noor Rain A, Badrul A, Adlin A, Norazah A, Zakiah I. In vitro screening of five local medicinal plants for antibacterial activity using disc diffusion method. *Trop Biomed*. 2005;22(2):165–70.

## Publisher's note

Springer Nature remains neutral with regard to jurisdictional claims in published maps and institutional affiliations.